Efficient Colorimetric pH Sensor Based on Responsive Polymer–Quantum Dot Integrated Graphene Oxide

Kwanyeol Paek, Hyunseung Yang, Junhyuk Lee, Junwoo Park, and Bumjoon J. Kim*

Department of Chemical and Biomolecular Engineering, Korea Advanced Institute of Science and Technology (KAIST), Daejeon 305-701, Republic of Korea

ABSTRACT In this paper, we report the development of a versatile platform for a highly efficient and stable graphene oxide (GO)-based optical sensor that exhibits distinctive ratiometric color responses. To demonstrate the applicability of the platform, we fabricated a colorimetric, GO-based pH sensor that responds to a wide range of pH changes. Our sensing system is based on responsive polymer and quantum dot (QD) hybrids integrated on a single GO sheet (MQD-GO), with the GO providing an excellent signal-to-noise ratio and high dispersion stability in water. The photoluminescence emissions of the blue and orange color-emitting QDs (BQDs and OQDs) in MQD-GO can be controlled independently by different pH-responsive linkers of poly(acrylic acid) (PAA) ($pK_a = 4.5$) and poly(2-vinylpyridine) (P2VP) ($pK_a = 3.0$) that can tune the efficiencies of Förster resonance energy transfer from the BQDs to the GO and from the OQDs to the GO, respectively. As a result, the color of MQD-GO changes from orange to near-white to blue over a wide range of pH values. The detailed mechanism of the pH-dependent response of the MQD-GO sensor was elucidated by measurements of time-resolved fluorescence and dynamic light scattering. Furthermore, the MQD-GO sensor showed excellent reversibility and high dispersion stability in pure water, indicating that our system is an ideal platform for biological and environmental applications. Our colorimetric GO-based optical sensor can be expanded easily to various other multifunctional, GO-based sensors by using alternate stimuli-responsive polymers.

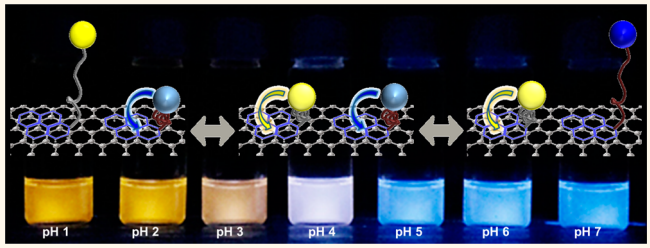

KEYWORDS: colorimetric sensor · pH sensor · graphene oxide · responsive polymer · quantum dot

Optical sensors based on fluorescence materials offer many advantages over conventional electrochemical approaches, including high sensitivity and ease of detection with the naked eye.[1−3] In recent years, stimuli-responsive polymer-based optical sensors have attracted great attention due to their fast response time and reversible changes in the conformations of the polymers.[4−7] Particularly, the polymer-based optical sensors were mainly focused on pH and a temperature sensing system using polymeric micelles[8−12] and nanoparticle−polymer hybrids[11,13−16] because the pH and temperature are basic target parameters in a broad range of applications from environmental to biomedical.[17] However, they often lack the ability to sense response over a wide range of pH and temperature responses. Also, they suffered from poor dispersion stability in aqueous media, resulting from their hydrophobic property when the polymers collapse during conformational changes.[18]

Graphene oxide (GO) has been identified as a promising sensing platform for stimuli-responsive polymer-based optical sensor applications because of its excellent potential in the highly sensitive Förster resonance energy transfer (FRET) acceptor, and, hence, it provides a high signal-to-noise ratio.[19−21] Also, GO has a high long-distance energy transfer rate because its rate is inversely proportional to the fourth power of the distance, which is a much weaker dependence on the distance than other FRET acceptors, including C_{60} and carbon nanotubes.[19,22−25] In addition, the large surface area of the GO provides excellent dispersion behavior in water. The surface properties and functionalities of GO can be tailored easily by anchoring nanoparticles and polymers *via* chemical and physical interactions, such as electrostatic, cycloaddition, hydrophobic, and $\pi-\pi$ stacking interactions.[26−33] These superior properties of GO can be combined to provide an ideal platform for pH sensors with long-term stability.

* Address correspondence to bumjoonkim@kaist.ac.kr.

Received for review December 30, 2013 and accepted February 18, 2014.

Published online February 18, 2014
10.1021/nn406657b

However, most GO-based sensors that have been developed to date respond to stimuli by exhibiting single photoluminescence (PL) intensity-based switching behavior that requires a specific detector to monitor the external changes effectively. Therefore, colorimetric detection methods are required for rapidly readable responses by using a simple detection approach, such as color change in the visible regime that can be detected by the naked eye.

A colorimetric sensor requires two or more fluorescent chromophores that emit different colors with strong luminescence. Semiconducting quantum dots (QDs) are promising candidates for the development of colorimetric sensors due to their size-dependent PL emissions, high quantum yield, and multiple emissions with a single light source.[34−38] In this regard, a series of single PL intensity-based QD-anchored GO-based optical sensors with sensing elements, such as the molecular beacon, chitosan, and poly(aniline), have been reported.[39,40] However, examples of GO-based colorimetric sensors are very limited.[41,42] Herein, we developed a versatile platform for an efficient GO-based optical sensor that exhibits distinctive ratiometric color responses. To demonstrate the applicability of the platform, we fabricated a colorimetric GO-based pH sensor that responds to a wide range of pH changes. A key strategy for generating a colorimetric, wide pH range sensor is to use two different blue- and orange-colored QDs anchored to a single GO sheet. The pH-dependent emissions of the blue and orange QDs were controlled by using linkers of two different pH-responsive polymers that changed their conformation in response to a different, but complementary, range of pH values. In addition, our GO-based sensor exhibits excellent dispersion stability in aqueous media and reversibility, all of which satisfy the critical requirements for a pH sensor.

RESULTS AND DISCUSSION

Figure 1 shows our key strategy and the components for producing a GO-based colorimetric pH sensor. Two different pH-responsive polymers, namely, poly(acrylic acid) (PAA) and poly(2-vinylpyridine) (P2VP), were chosen as linkers between the GO and the QDs to generate responses over a wide range of pH values. The PAA chains were grafted onto the surface of the blue-colored cadmium sulfide/zinc sulfide QDs (BQDs), and the P2VP polymers were grafted onto the surface of the orange-colored cadmium selenide/zinc sulfide QDs (OQDs). The PAA-coated BQDs (PAA-BQDs) and P2VP-coated OQDs (P2VP-OQDs) were integrated simultaneously on the surface of single GO sheet (mixed PAA-BQD and P2VP-OQD anchored GO, MQD-GO) by $\pi-\pi$ stacking interactions between the pyrene functional groups on the PAA and P2VP chains and the basal plane of the GO surfaces. (Synthesis details are provided in the Methods section.) The PAA chains respond to changes in their chain conformation in the pK_a around pH 4.5 due to the ionization of the carboxylic acid groups.[43] Conversely, the P2VP polymers exhibit coil−globule transition at their pK_a around pH 3.0 due to the protonation of amine groups in acidic pH.[14,44] Therefore, the PL emissions of the BQDs and OQDs in MQD-GO can be controlled independently by the conformational transitions of two different PAA and P2VP chains at their corresponding pK_a values since the FRET efficiency is governed by the distance between the FRET donor (QD) and acceptor (GO).[14] It was observed that the color of MQD-GO changes from orange to white to blue as the pH of the solution increases from 1 to 7.

Scheme S1 (Supporting Information) presents a synthesis procedure for pH-responsive P2VP (4) and PAA (7) polymers, both of which have two functional end groups of pyrene and thiol. First, the pyrene was introduced at the end of the reversible addition−fragmentation chain transfer (RAFT) agent (1) to

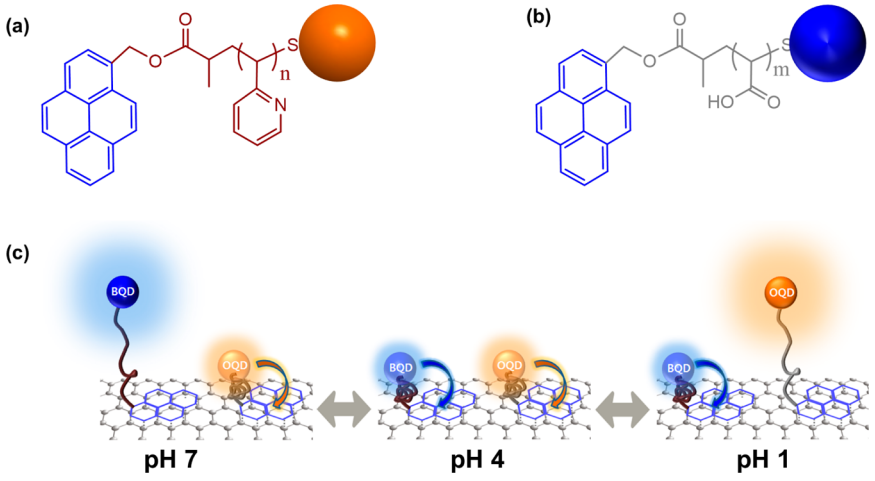

Figure 1. Structure of (a) P2VP-OQD and (b) PAA-BQD. (c) Schematic illustration of the conformation and behavior of MQD-GO at a given pH value.

produce a pyrene terminal group at the one end of the P2VP and PAA chains because the pyrene-terminated polymers can be anchored easily to the GO surface by the strong interaction of $\pi-\pi$ stacking.[45−47] The polymers were synthesized by RAFT polymerization to precisely control their molecular weights (M_n) within a narrow polydispersity index (PDI) number. The M_n of the polymer is a critical parameter that can determine the FRET efficiencies of the BQDs and OQDs to GO.[33] Therefore, we carefully chose and synthesized the desired M_n values of PAA and P2VP. In this work, the M_n and PDI of PAA were 10.4 kg/mol and 1.15, respectively, while these values for the P2VP were 14.4 kg/mol and 1.27, respectively (Figure S1). Finally, the opposite ends of the polymer chains were functionalized with thiol groups by reaction with hexylamine for further ligand exchange reaction with the QDs. On the other hand, two types of different-colored QDs (*i.e.*, BQDs emitting at 440 nm and OQDs emitting at 580 nm) were synthesized by the one-step, chemical composition-gradients method that uses oleic acid (OA) for stabilization (Figure S2).[48,49] Subsequently, the surfaces of the OQDs and BQDs were modified with the thiol-terminated P2VP (4) and PAA (7), respectively, *via* ligand exchange. Thus, the as-synthesized OA-coated QDs were dispersible only in organic solvents (Figure S2), whereas PAA-BQDs and P2VP-OQDs were easily dispersible in aqueous solvents after ligand exchange (Figure S3). The successful preparation of PAA-BQDs was evidenced by their PL spectra, which showed multiple emission peaks from pyrene end functional groups of PAA chains at 417 and 470 nm and BQDs at 440 nm.[50] In addition, P2VP-OQDs exhibited multiple emission peaks at 417, 470, and 580 nm, with the characteristic peak of the OQDs located at 580 nm. Hence, the TEM and PL results indicated that the PAA and P2VP chains were grafted successfully onto the surfaces of the BQDs and OQDs, respectively.

GO was synthesized using the improved Hummers method.[51] Subsequently, the PAA-BQDs and P2VP-OQDs were anchored onto the surface of the GO by using $\pi-\pi$ stacking. Figure S5 compares the attenuated total reflectance Fourier transform infrared (ATR-FTIR) spectrum of MQD-GO with those of GO, P2VP-OQD, and PAA-BQD. The MQD-GO sample had intense peaks around 2350 cm^{-1}, indicating that PAA-BQD and P2VP-OQD were anchored to the GO surface by the $\pi-\pi$ stacking reaction.[52] This noncovalent immobilization can be achieved at mild conditions without involving any high-temperature reactions, and there should be no damage to the materials during the reaction. Thus, our method using pyrene-functionalized RAFT agents provides a simple, two-step reaction process for developing polymer−GO hybrids, and this process can be extended easily to other polymer-grafting methods.[53,54] The ratio of PAA-BQDs to P2VP-OQDs in MQD-GO during the grafting reaction was kept at 1:1 to obtain a balanced, near-white color. Single-type QD-anchored GOs that contained either PAA-BQD or P2VP-OQD (BQD-PAA-GO and OQD-P2VP-GO) also were prepared for use as control samples. Any ungrafted QDs were thoroughly removed *via* repeated centrifugation at 13 500 rpm and decantation. Figure 2a−c shows the TEM images of BQD-PAA-GO, OQD-P2VP-GO, and

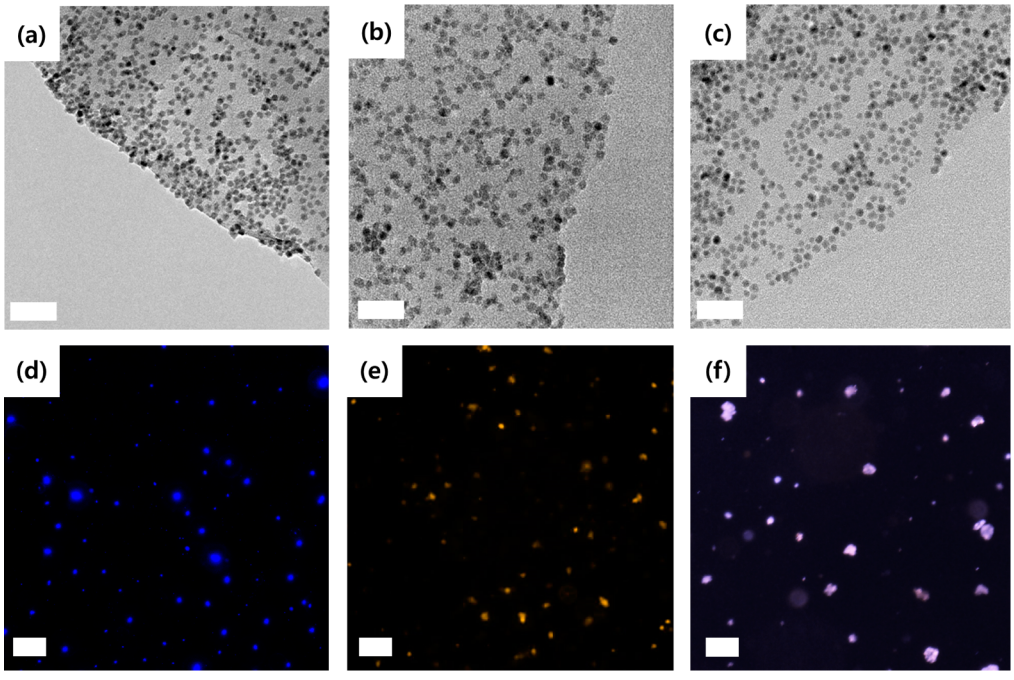

Figure 2. TEM and fluorescence microscopy images of (a,d) BQD-PAA-GO, (b,e) OQD-P2VP-GO, and (c,f) MQD-GO. The scale bar is 50 nm for TEM and 25 μm for the fluorescence microscopy images. The fluorescence microscopy images were obtained at pH 7 for (d) BQD-PAA-GO, (e) pH 1 for OQD-P2VP-GO, and (f) pH 4 for MQD-GO.

MQD-GO, while Figure 2d–f presents their corresponding fluorescence microscopy images measured at optimized pH conditions, that is, pH 7 for BQD-PAA-GO, pH 1 for OQD-P2VP-GQ, and pH 4 for MQD-GO, for comparing the colors they emitted. It was obvious from the TEM analysis that, for all three samples, the QDs were homogeneously and densely distributed over the entire surface of the GO, including the edges and basal planes without any aggregation. Interestingly, the dot-patterned blue and orange luminescence in Figure 2d,e originated from the BQD-PAA-GO and OQD-P2VP-GO, indicating that pyrene-terminated PAA-BQDs and P2VP-OQDs were anchored successfully onto the GO surface with complete removal of ungrafted PAA-BQDs and P2VP-OQDs. The fluorescence microscopy image of MQD-GO in pH 4 buffer solution exhibited the mixed colored dot patterns from the combined emissions of BQDs and OQDs on a single GO sheet. Therefore, the combined features from TEM, fluorescence microscopy, and ATR-FTIR confirmed the successful preparation of the MQD-GO.

Figure 3a shows the PL spectra of MQD-GO in aqueous media at different pH conditions; these spectra were obtained after irradiating the solution at 365 nm. The concentration of MQD-GO was maintained at 1.0 mg mL^{-1} to avoid any PL quenching of the QDs by other GO sheets in the solution. The PL spectra of MQD-GO exhibited two emission peaks, one at 440 nm from BQD and the other one at 580 nm from OQD. The pyrene emissions at 410 and 470 nm completely disappeared because the photo-excited electrons in the pyrene were transferred effectively to the empty electronic states of the adjacent GO. This feature provides additional evidence of the successful anchoring of the pyrene-terminated P2VP-OQDs and PAA-BQDs to the GO.[55,56] The PL intensity of MQD-GO at 440 nm increased gradually as the pH value of the solution increased from pH 4 to 7, and the PL peak at 440 nm reached saturation above pH 7. In contrast, the PL intensity of MQD-GO at 580 nm gradually decreased as the pH value of the solution increased from 1 to 5. At pH 5, the peak at 580 nm reached saturation. The MQD-GO solution exhibited no change in color below pH 1 or above pH 7. To quantitatively determine whether the pH-dependent change in the emission spectra could be used for accurate pH sensing, the PL intensity ratio at the different emission levels of 580 and 440 nm (I_{580nm}/I_{440nm}) was compared and plotted as a function of pH in Figure 3b. Interestingly, the plot of pH *versus* I_{580nm}/I_{440nm} became almost linear in the pH range of 2–5, indicating that the response was ratiometric in this range. This behavior of the PL spectra can be highlighted in the color changes of the MQD-GO solution as the pH values changed, as shown in Figure 3c. At the low pH value of 1, the color of the solution was dominated by the orange emission at 580 nm. In contrast, the color of the MQD-GO solution at pH 7 was blue because of the dominant emission at 440 nm. The balanced emissions from both the QDs at pH 4 are responsible for a near-white color solution. These results can be explained well by the pH-dependent conformation changes of PAA and P2VP polymers that determine the distance between the QDs and the GO surface. Because the

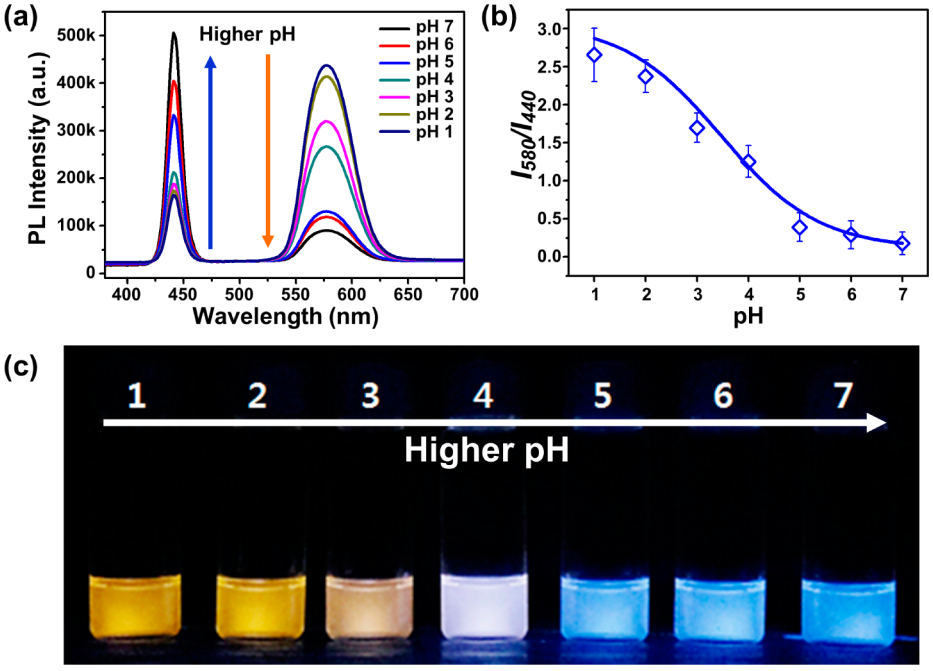

Figure 3. (a) PL spectra of MQD-GO as a function of pH value under irradiation at 365 nm; (b) PL intensity changes (I_{580}/I_{440}) as a function of pH; (c) photographic images of MQD-GO in buffer solutions with the indicated pH values under irradiation at 365 nm.

FRET efficiency is inversely proportional to the fourth power of the FRET donor-to-acceptor separation distance when GO acts as a FRET acceptor,[19,22] the separation distance between the QDs and the GO is a key parameter in controlling the pH-dependent PL spectra and the color of MQD-GO in solution. Because the pK_a value of P2VP is around 3, the P2VP chains were protonated and swollen by water below pH 3. When the pK_a value of PAA was around 4.5, the PAA chains became ionized and soluble in water above pH 4.5. Therefore, when the pH is greater than 4.5, the PAA chain has an extended conformation so that the BQDs and GO are farther apart, whereas most of the orange emission of the OQDs becomes quenched by the GO due to the collapsed conformation of the P2VP chains. In contrast, when the pH is below 3, the PAA chains still remain in the collapsed conformation, whereas P2VP has an extended conformation, so the OQDs are positioned far enough from the GO to suppress the FRET from the OQDs and induce a strong orange emission. Finally, when the pH was less than the pK_a of PAA but greater than the pK_a of P2VP, both PAA and P2VP chains collapsed to intermediate conformations, thus affording the balanced colors combined from the emissions of both the BQDs and OQDs.

The effect of the sizes of the PAA-BQD and P2VP-OQD particles on changes in the pH value was measured by dynamic light scattering (DLS) to elucidate the effect of the conformational changes of PAA and P2VP on the pH response of the MQD-GOs (Figure S6). Although DLS measures the hydrodynamic sizes of the particles that can be overestimated due to the swelling of the polymer chains by the solvent, comparing the measured particle sizes to changes in the pH should provide useful information on the pH-dependent conformations of the PAA and P2VP spacers and, thus, the pH-dependent PL spectra of the MQD-GO.[57,58] The hydrodynamic size of the PAA-BQD decreased from approximately 70 to 30 nm when pH changed from 7 to 4, and saturation occurred at pH 4. Conversely, the hydrodynamic size of P2VP-OQD was unchanged above pH 4, but it increased dramatically from 45 to 85 nm as pH was decreased from 4 to 1. The pH values for the size transition of PAA-BQD and P2VP-OQD clearly can explain the transitions in the PL intensities of BQD-PAA-GO, OQD-P2VP-GO (Figure S7), and MQD-GO (Figure 3). For example, as the pH decreases from 4 to 1, the P2VP chains were swelled by water, increasing the size of the P2VP-OQDs and the distance between the donor and the acceptor. The corresponding decrease in the FRET efficiency results in an increase in the PL intensity of OQDs in the MQD-GO. Conversely, the P2VP polymers were fully deprotonated above pH 4, and the corresponding particle size was unchanged.

A deeper insight into the change in PL and color spectra of MQD-GO can be obtained by quantitative comparison of the average fluorescence lifetime (τ_{ave}) of the BQDs and OQDs in MQD-GO solution under different pH conditions. The fluorescent decay of the BQDs and OQDs of MQD-GO was investigated by time-resolved fluorescence (TRF) measurements with filtering at 440 nm for BQDs and at 580 nm for OQD under irradiation at 370 nm. FRET occurs when energy is transferred nonradiatively from the donor to the acceptor, and the efficiency of this transfer can be monitored by the change in the τ_{ave} value of the fluorophores.[59,60] For example, when the distance between the QDs and GO becomes shorter by the conformational changes of the polymer, the average lifetime of FRET will decrease.[21] The TRF curves of MQD-GO were also pH-sensitive, exhibiting multi-exponential decay due to the dynamic quenching between the QDs and GO.[21,61] The best fits for both series of TRF curves at 440 and 580 nm were obtained using a double-exponential decay model (Figure 4a,b), and the results are summarized in Table S1. At pH 1, the OQDs in the MQD-GO samples had a τ_{ave} value of 11.59 ns, with two decay components of 0.30 ns (22.06%) and 14.79 ns (77.94%). At the greater pH value of 4, the OQDs' decay process was much faster, with a τ_{ave} value of 5.33 ns, with decay components of 0.22 ns (61.25%) and 13.42 ns (38.75%). The shorter lifetime of the OQDs in the MQD-GO was attributed to an increase in the nonradiative decay rate caused by energy transfer from the OQD to the GO. Interestingly, at the intermediate pH regimes, the τ_{ave} values of the OQDs had a decreasing trend, that is, 11.31 ns (pH 2), 7.60 ns (pH 3), and 5.33 ns (pH 4). Finally, the τ_{ave} values of OQDs were saturated above pH 5. Therefore, the trend in the τ_{ave} value of the OQDs in the MQD-GO sample coincides excellently with those in the conformational changes of the P2VP spacer and in their PL spectra. A similar TRF trend was obtained for the BQDs in the MQD-GO sample in terms of the pK_a value of the PAA spacer. The τ_{ave} of the BQDs was 7.53 ns, with two decay components of 0.26 ns (79.30%) and 35.37 ns (20.70%) at pH 7. With the decrease in pH values, the τ_{ave} of the BQDs decreased remarkably and was saturated at 3.50 ns, with 0.15 ns (91.05%) and 31.98 ns (8.95%) at pH 4. Figure 4c presents the plots of the τ_{ave} changes *versus* pH values for two different BQDs and OQDs of the MQD-GOs. The TRF results indicated that the drastic change in the chain conformations of P2VP and PAA spacers occurred around their pK_a values. This feature generated pH-dependent changes in the FRET efficiencies from the QDs to the GO and the PL spectra and PL decay of MQD-GOs over a wide range of pH values.

The key requirements for practical application of optical sensors include good stability and reversibility. However, most polymer-based pH sensors in previous reports are not suitable for use in biological and environmentally friendly applications because of their

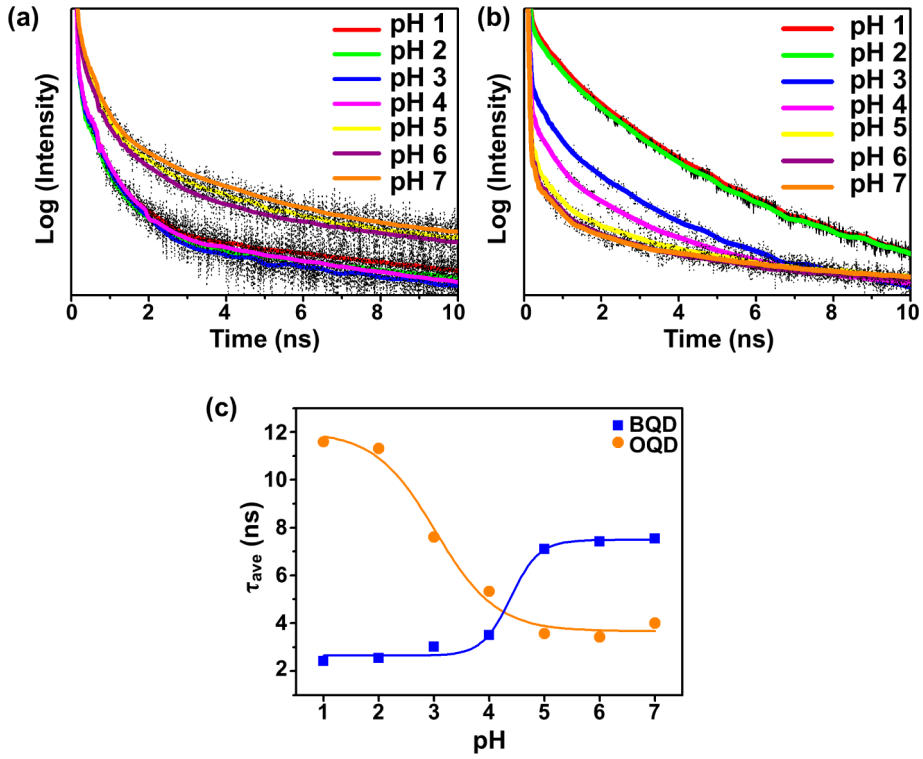

Figure 4. Time-resolved fluorescence (TRF) spectra of MQD-GO at various pH values: TRF was measured for the MQD-GO at the given pH with filtering (a) 440 nm for BQDs and (b) 580 nm for OQDs under irradiation at 370 nm. The fitting curve was obtained using a double-exponential decay model. (c) Plot of τ_{ave} values of BQDs and OQDs *vs* pH variation.

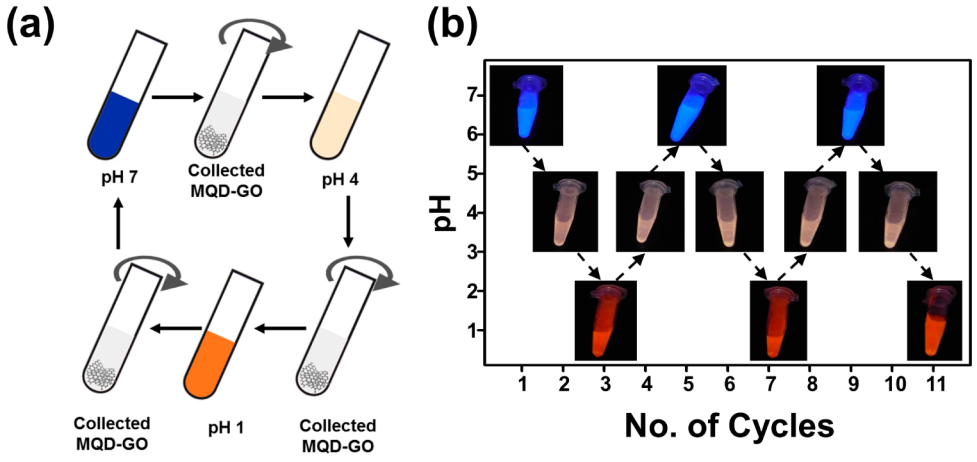

Figure 5. (a) Schematic illustration. (b) Reversibility test of MQD-GO for several cycles: MQD-GO in aqueous media at a given pH was collected by centrifugation at 13 500 rpm for 5 min and subsequently dispersed in aqueous media with different pH value. The photographic images of the MQD-GO solution were obtained at 365 nm irradiation using a UV lamp.

poor dispersion stability in water. When polymers are in the collapsed conformation in response to pH change, the hydrophobic nature of the polymer chains typically causes poor dispersion of the sensors in aqueous media. Therefore, previous sensors either had to operate in a solvent system that consisted of water mixed with some organic solvents or required the introduction of water-soluble derivatives, such as poly(ethylene glycol), in order to improve their solubility in water.[14,18] In contrast, our MQD-GO can fully exploit the advantage of the water-soluble GO platform without any other external agents, and it exhibits high dispersion stability in water and high reversibility. Figure 5 shows the continuous cycles of the MQD-GO in aqueous media with varying pH values to ensure the reversibility of the sensor. The MQD-GO was first dispersed in pH 7 buffer solution, and the blue color appeared. Subsequently, the resulting blue solution was collected by centrifugation and dispersed in a pH 4 buffer solution. This generated an immediate color change of the MQD-GO solution to a near-white color. When the MQD-GO was recycled by

centrifugation and subsequently dispersed in pH 1 buffer solution, the color of the MQD-GO changed to orange. This procedure can be repeated many times, demonstrating the excellent reversibility of the MQD-GO sensor.

CONCLUSIONS

We developed a versatile platform for a highly stable, colorimetric, wide-range pH sensor. This pH sensor consists of responsive polymer and QD hybrids integrated onto the surface of GO. The distances between the two color-emitting QDs and the GO were controlled independently *via* two linkers of pH-responsive PAA and P2VP, resulting in colorimetric responses over a wide range of pH values. In addition, our pH sensor exhibited excellent reversibility in aqueous media, which benefitted from the use of GO platform. Our novel platform can be applied to various sensor systems with alternate stimuli, such as temperature, light, ions, and redox reactions, thus allowing promising opportunities for use in environmental and biological applications.

METHODS

Synthesis of Pyrene-Functionalized RAFT Chain Transfer Agent (2). The trithiocarbonate RAFT chain transfer agent (**1**) was synthesized according to methods provided in the literature.[14,62−64] The pyrene-functionalized RAFT agent was synthesized *via* a *N*,*N*′-dicyclohexylcarbodiimide (DCC) coupling reaction. Briefly, 16.7 mmol of trithiocarbonate RAFT agent (**1**), 33.4 mmol of 1-pyrenemethanol, and 8.4 mmol of 4-dimethylaminopyridine (DMAP) were mixed in 200 mL of dichloromethane (DCM). After 15 min, 16.7 mmol of DCC in 20 mL of DCM was added to the mixture, and the color of the solution changed from red to dark yellow. After 36 h, the mixture was filtered, and the solvent was evaporated. The crude products were purified through column chromatography (hexane/toluene). Finally, a dark yellow powder was obtained. ^{1}H NMR ($CDCl_3$, 500 MHz): δ 8.0−8.32 (m, 9H), 5.89 (s, 2H), 4.86 (q, J = 7.4 Hz, 1H), 3.22 (t, J = 7.4 Hz, 2H), 1.59 (d, J = 7.3 Hz, 3H), 1.52−1.59 (m, 2H), 1.27−1.35 (m, 2H), 0.89 (t, J = 7.4 Hz, 3H).

Synthesis of Pyrene-Functionalized P2VP (4) and PAA (7). For P2VP polymer (**3**), the 2-vinylpyridine monomer, pyrene-functionalized RAFT agent (**2**), and azobisisobutyronitrile (AIBN) were added into a glass ampule, and subsequently, the mixture was degassed and heated to 70 °C for 12 h. Then, the synthesized P2VP (**3**) was precipitated by hexane. The PAA was synthesized from poly(*tert*-butyl acrylate) (PtBA). For PtBA polymer (**5**), *tert*-butyl acrylate monomer, pyrene-functionalized RAFT agent (**2**), and AIBN were added into a glass ampule, and the mixture was degassed and heated to 70 °C for 2 h. The product was dissolved in THF and precipitated in water. The end groups of P2VP (**3**) and PtBA (**5**) were converted to thiol groups by reaction with hexylamine for further ligand exchange reaction with the QDs. The *tert*-butyl ester groups on PtBA (**6**) were hydrolyzed by using excess trifluoroacetic acid (TFA), and then the hydrolyzed PAA (**7**) was precipitated using DCM.

Synthesis of PAA-BQD and P2VP-OQD. OA-coated BQDs and OQDs were synthesized *via* the previously reported, one-pot, composition chemical gradients method.[48,49] The surfaces of the BQDs and OQDs, which were coated with the OA ligands, were substituted by thiol-terminated PAA and P2VP chains in THF and precipitated with hexane, respectively. Finally, those QDs were redispersed in methanol and washed by membrane filtration (Millipore Amicon Ultra) to remove ungrafted polymers.

Preparation of MQD-GO. GO was prepared using the improved Hummers method.[51] To prepare MQD-GO, 10 mg of GO, 50 mg of PAA-BQD, and 50 mg of P2VP-OQD in dimethylformamide (DMF) were placed in a flask. A flow of argon was bubbled through the solution for 1 h before the reaction, and the mixture was stirred at room temperature for 2 days. Then, the mixture was purified by repeated centrifugation and decantation in DMF at 13 500 rpm for 5 min to remove ungrafted PAA-BQD and P2VP-OQD.

Characterization of MQD-GO. The structural analysis of the materials used in this study was performed by ^{1}H nuclear magnetic resonance (NMR, Bruker AMX 500) and size exclusion chromatography (SEC, Waters 1515) equipped with a differential refractometer (Waters 2414) with THF as the eluent at a flow rate of 1 mL/min; the column was calibrated using polystyrene (PS) standards. ATR-FTIR spectra were taken using a Bruker ALPHA. TEM (JEOL-2000FX) was used to observe the surfaces and the internal structures of the MQD-GO. Fluorescence images were obtained by a fluorescence optical microscope (Nikon Eclipse Ti-U) using a single UV source. PL spectra and fluorescence lifetimes were obtained from a Horiba Jobin Yvon NanoLog spectrophotometer. The excitation wavelength was set at 365 nm, and a 10 mm quartz cuvette was used for the PL spectra. Fluorescence lifetimes were measured using a NanoLED laser light source at 370 nm for the excitation, and the emissions were collected at 440 and 580 nm. The data were fitted by a double-exponential decay model. The samples for the PL measurements were prepared by dissolving MQD-GO in a buffer solution at very low concentrations (1.0 mg/mL). The hydrodynamic sizes of the PAA-BQD and P2VP-OQD at given pH values were determined *via* DLS measurements using a Malvern Zetasizer Nano ZS. The optical properties were measured using a Shimadzu UV spectrophotometer (UV-1800).

Conflict of Interest: The authors declare no competing financial interest.

Acknowledgment. This research was supported by the Korea Research Foundation Grant funded by the Korean Government (2013R1A2A1A03069803). We thank Soojeong Cho for the help in the fluorescence optical microscopy measurements. We also thank Dr. Tharangattu N. Narayanan and Prof. Luis Campos for useful discussions.

Supporting Information Available: Additional characterization data (SEC, PL, UV−vis, TEM, TRF, and DLS data) and synthetic scheme of the synthesized materials. This material is available free of charge *via* the Internet at http://pubs.acs.org.

REFERENCES AND NOTES

1. Somers, R. C.; Bawendi, M. G.; Nocera, D. G. CdSe Nanocrystal Based Chem-/Bio-Sensors. *Chem. Soc. Rev.* **2007**, *36*, 579–591.
2. Basabe-Desmonts, L.; Reinhoudt, D. N.; Crego-Calama, M. Design of Fluorescent Materials for Chemical Sensing. *Chem. Soc. Rev.* **2007**, *36*, 993–1017.
3. Kermis, H. R.; Kostov, Y.; Harms, P.; Rao, G. Dual Excitation Ratiometric Fluorescent pH Sensor for Noninvasive Bioprocess Monitoring: Development and Application. *Biotechnol. Prog.* **2002**, *18*, 1047–1053.
4. Stuart, M. A. C.; Huck, W. T. S.; Genzer, J.; Muller, M.; Ober, C.; Stamm, M.; Sukhorukov, G. B.; Szleifer, I.; Tsukruk, V. V.; Urban, M.; *et al.* Emerging Applications of Stimuli-Responsive Polymer Materials. *Nat. Mater.* **2010**, *9*, 101–113.
5. Hu, J.; Liu, S. Responsive Polymers for Detection and Sensing Applications: Current Status and Future Developments. *Macromolecules* **2010**, *43*, 8315–8330.
6. Pietsch, C.; Hoogenboom, R.; Schubert, U. S. Soluble Polymeric Dual Sensor for Temperature and pH Value. *Angew. Chem., Int. Ed.* **2009**, *48*, 5653–5656.

7. Wu, T.; Zou, G.; Hu, J.; Liu, S. Fabrication of Photoswitchable and Thermotunable Multicolor Fluorescent Hybrid Silica Nanoparticles Coated with Dye-Labeled Poly(*N*-isopropylacrylamide) Brushes. *Chem. Mater.* **2009**, *21*, 3788–3798.
8. Li, C.; Zhang, Y.; Hu, J.; Cheng, J.; Liu, S. Reversible Three-State Switching of Multicolor Fluorescence Emission by Multiple Stimuli Modulated FRET Processes within Thermoresponsive Polymeric Micelles. *Angew. Chem., Int. Ed.* **2010**, *49*, 5120–5124.
9. Kumar, E. K. P.; Fedborg, L. N.; Almdal, K.; Andresen, T. L. Synthesis and Characterization of a Micelle-Based pH Nanosensor with an Unprecedented Broad Measurement Range. *Chem. Mater.* **2013**, *25*, 1496–1501.
10. Lee, A. S.; Gast, A. P.; Bütün, V.; Armes, S. P. Characterizing the Structure of pH Dependent Polyelectrolyte Block Copolymer Micelles. *Macromolecules* **1999**, *32*, 4302–4310.
11. Gao, G. H.; Im, G. H.; Kim, M. S.; Lee, J. W.; Yang, J.; Jeon, H.; Lee, J. H.; Lee, D. S. Magnetite-Nanoparticle-Encapsulated pH-Responsive Polymeric Micelle as an MRI Probe for Detecting Acidic Pathologic Areas. *Small* **2010**, *6*, 1201–1204.
12. Bae, Y.; Fukushima, S.; Harada, A.; Kataoka, K. Design of Environment-Sensitive Supramolecular Assemblies for Intracellular Drug Delivery: Polymeric Micelles That Are Responsive to Intracellular pH Change. *Angew. Chem., Int. Ed.* **2003**, *42*, 4640–4643.
13. Hong, S. H.; Hong, S. W.; Jo, W. H. A New Polymeric pH Sensor Based on Photophysical Property of Gold Nanoparticle and pH Sensitivity of Poly(sulfadimethoxine methacrylate). *Macromol. Chem. Phys.* **2010**, *211*, 1054–1060.
14. Paek, K.; Chung, S.; Cho, C. H.; Kim, B. J. Fluorescent and pH-Responsive Diblock Copolymer-Coated Core−Shell CdSe/ZnS Particles for a Color-Displaying, Ratiometric pH Sensor. *Chem. Commun.* **2011**, *47*, 10272–10274.
15. Kozlovskaya, V.; Kharlampieva, E.; Chang, S.; Muhlbauer, R.; Tsukruk, V. V. pH-Responsive Layered Hydrogel Microcapsules as Gold Nanoreactors. *Chem. Mater.* **2009**, *21*, 2158–2167.
16. Medintz, I. L.; Stewart, M. H.; Trammell, S. A.; Susumu, K.; Delehanty, J. B.; Mei, B. C.; Melinger, J. S.; Blanco-Canosa, J. B.; Dawson, P. E.; Mattoussi, H. Quantum-Dot/Dopamine Bioconjugates Function as Redox Coupled Assemblies for *In Vitro* and Intracellular pH Sensing. *Nat. Mater.* **2010**, *9*, 676–684.
17. Wencel, D.; Abel, T.; McDonagh, C. Optical Chemical pH Sensors. *Anal. Chem.* **2014**, *86*, 15–29.
18. Hong, S. W.; Ahn, C. H.; Huh, J.; Jo, W. H. Synthesis of a PEGylated Polymeric pH Sensor and Its pH Sensitivity by Fluorescence Resonance Energy Transfer. *Macromolecules* **2006**, *39*, 7694–7700.
19. Swathi, R. S.; Sebastian, K. L. Long Range Resonance Energy Transfer from a Dye Molecule to Graphene Has (Distance)(−4) Dependence. *J. Chem. Phys.* **2009**, *130*, 086101.
20. Liu, C.; Wang, Z.; Jia, H.; Li, Z. Efficient Fluorescence Resonance Energy Transfer between Upconversion Nanophosphors and Graphene Oxide: A Highly Sensitive Biosensing Platform. *Chem. Commun.* **2011**, *47*, 4661–4663.
21. Huang, P. -J. J.; Liu, J. DNA-Length-Dependent Fluorescence Signaling on Graphene Oxide Surface. *Small* **2012**, *8*, 977–983.
22. Zhang, C.; Yuan, Y.; Zhang, S.; Wang, Y.; Liu, Z. Biosensing Platform Based on Fluorescence Resonance Energy Transfer from Upconverting Nanocrystals to Graphene Oxide. *Angew. Chem., Int. Ed.* **2011**, *50*, 6851–6854.
23. Stewart, M. H.; Huston, A. L.; Scott, A. M.; Oh, E.; Algar, W. R.; Deschamps, J. R.; Susumu, K.; Jain, V.; Prasuhn, D. E.; Blanco-Canosa, J.; *et al.* Competition between Forster Resonance Energy Transfer and Electron Transfer in Stoichiometrically Assembled Semiconductor Quantum Dot-Fullerene Conjugates. *ACS Nano* **2013**, *7*, 9489–9505.
24. Morales-Narvaez, E.; Perez-Lopez, B.; Pires, L. B.; Merkoci, A. Simple Forster Resonance Energy Transfer Evidence for the Ultrahigh Quantum Dot Quenching Efficiency by Graphene Oxide Compared to Other Carbon Structures. *Carbon* **2012**, *50*, 2987–2993.
25. Chen, Z.; Berciaud, S.; Nuckolls, C.; Heinz, T. F.; Brus, L. E. Energy Transfer from Individual Semiconductor Nanocrystals to Graphene. *ACS Nano* **2010**, *4*, 2964–2968.
26. Zheng, Z.; Zheng, X.; Wang, H.; Du, Q. Macroporous Graphene Oxide−Polymer Composite Prepared through Pickering High Internal Phase Emulsions. *ACS Appl. Mater. Interfaces* **2013**, *5*, 7974–7982.
27. Narayanan, T. N.; Gupta, B. K.; Vithayathil, S. A.; Aburto, R. R.; Mani, S. A.; Taha-Tijerina, J.; Xie, B.; Kaipparettu, B. A.; Torti, S. V.; Ajayan, P. M. Hybrid 2D Nanomaterials as Dual-Mode Contrast Agents in Cellular Imaging. *Adv. Mater.* **2012**, *24*, 2992–2998.
28. Yang, H.; Kwon, Y.; Kwon, T.; Lee, H.; Kim, B. J. 'Click' Preparation of CuPt Nanorod-Anchored Graphene Oxide as a Catalyst in Water. *Small* **2012**, *8*, 3161–3168.
29. Zhang, Y.; Zhang, J.; Huang, X.; Zhou, X.; Wu, H.; Guo, S. Assembly of Graphene Oxide-Enzyme Conjugates through Hydrophobic Interaction. *Small* **2012**, *8*, 154–159.
30. Yang, X.; Zhang, X.; Liu, Z.; Ma, Y.; Huang, Y.; Chen, Y. High-Efficiency Loading and Controlled Release of Doxorubicin Hydrochloride on Graphene Oxide. *J. Phys. Chem. C* **2008**, *112*, 17554–17558.
31. Pan, Y.; Bao, H.; Sahoo, N. G.; Wu, T.; Li, L. Water-Soluble Poly(*N*-isopropylacrylamide)−Graphene Sheets Synthesized *via* Click Chemistry for Drug Delivery. *Adv. Funct. Mater.* **2011**, *21*, 2754–2763.
32. Zhang, L.; Xia, J.; Zhao, Q.; Liu, L.; Zhang, Z. Functional Graphene Oxide as a Nanocarrier for Controlled Loading and Targeted Delivery of Mixed Anticancer Drugs. *Small* **2010**, *6*, 537–544.
33. Yang, H.; Paek, K.; Kim, B. J. Efficient Temperature Sensing Platform Based on Fluorescent Block Copolymer-Functionalized Graphene Oxide. *Nanoscale* **2013**, *5*, 5720–5724.
34. Shirasaki, Y.; Supran, G. J.; Bawendi, M. G.; Bulovic, V. Emergence of Colloidal Quantum-Dot Light-Emitting Technologies. *Nat. Photonics* **2013**, *7*, 13–23.
35. Sukhovatkin, V.; Hinds, S.; Brzozowski, L.; Sargent, E. H. Colloidal Quantum-Dot Photodetectors Exploiting Multiexciton Generation. *Science* **2009**, *324*, 1542–1544.
36. Geyer, S. M.; Scherer, J. M.; Moloto, N.; Jaworski, F. B.; Bawendi, M. G. Efficient Luminescent Down-Shifting Detectors Based on Colloidal Quantum Dots for Dual-Band Detection Applications. *Acs Nano* **2011**, *5*, 5566–5571.
37. Murray, C. B.; Norris, D. J.; Bawendi, M. G. Synthesis and Characterization of Nearly Monodisperse CdE (E = S, Se, Te) Semiconductor Nanocrystallites. *J. Am. Chem. Soc.* **1993**, *115*, 8706–8715.
38. Alivisatos, A. P. Semiconductor Clusters, Nanocrystals, and Quantum Dots. *Science* **1996**, *271*, 933–937.
39. Dong, H.; Gao, W.; Yan, F.; Ji, H.; Ju, H. Fluorescence Resonance Energy Transfer between Quantum Dots and Graphene Oxide for Sensing Biomolecules. *Anal. Chem.* **2010**, *82*, 5511–5517.
40. Wang, T.; Zhang, S.; Mao, C.; Song, J.; Niu, H.; Jin, B.; Tian, Y. Enhanced Electrochemiluminescence of CdSe Quantum Dots Composited with Graphene Oxide and Chitosan for Sensitive Sensor. *Biosens. Bioelectron.* **2012**, *31*, 369–375.
41. Zhu, H.; Zhang, W.; Zhang, K.; Wang, S. Dual-Emission of a Fluorescent Graphene Oxide-Quantum Dot Nanohybrid for Sensitive and Selective Visual Sensor Applications Based on Ratiometric Fluorescence. *Nanotechnology* **2012**, *23*, 315502.
42. Wang, X.; Sun, X.; Hu, P. A.; Zhang, J.; Wang, L.; Feng, W.; Lei, S.; Yang, B.; Cao, W. Colorimetric Sensor Based on Self-Assembled Polydiacetylene/Graphene-Stacked Composite Film for Vapor-Phase Volatile Organic Compounds. *Adv. Funct. Mater.* **2013**, *23*, 6044–6050.
43. Schilli, C. M.; Zhang, M.; Rizzardo, E.; Thang, S. H.; Chong, Y. K.; Edwards, K.; Karlsson, G.; Muller, A. H. E. A New

Double-Responsive Block Copolymer Synthesized *via* RAFT Polymerization: Poly(*N*-isopropylacrylamide)-*block*-Poly(acrylic acid). *Macromolecules* **2004**, *37*, 7861–7866.
44. Hayward, R. C.; Chmelka, B. F.; Kramer, E. J. Crosslinked Poly(styrene)-*block*-Poly(2-vinylpyridine) Thin Films as Swellable Templates for Mesostructured Silica and Titania. *Adv. Mater.* **2005**, *17*, 2591–2595.
45. Pham, T. A.; Choi, B. C.; Jeong, Y. T. Facile Covalent Immobilization of Cadmium Sulfide Quantum Dots on Graphene Oxide Nanosheets: Preparation, Characterization, and Optical Properties. *Nanotechnology* **2010**, *21*, 465603.
46. Xu, Y. X.; Bai, H.; Lu, G.; Li, C.; Shi, G. Flexible Graphene Films *via* the Filtration of Water-Soluble Noncovalent Functionalized Graphene Sheets. *J. Am. Chem. Soc.* **2008**, *130*, 5856–5857.
47. Liu, J.; Yang, W.; Tao, L.; Li, D.; Boyer, C.; Davis, T. P. Thermosensitive Graphene Nanocomposites Formed Using Pyrene-Terminal Polymers Made by RAFT Polymerization. *J. Polym. Sci., Part A: Polym. Chem.* **2010**, *48*, 425–433.
48. Bae, W. K.; Nam, M. K.; Char, K.; Lee, S. Gram-Scale One-Pot Synthesis of Highly Luminescent Blue Emitting $Cd_{1-x}Zn_xS$/ZnS Nanocrystals. *Chem. Mater.* **2008**, *20*, 5307–5313.
49. Bae, W. K.; Char, K.; Hur, H.; Lee, S. Single-Step Synthesis of Quantum Dots with Chemical Composition Gradients. *Chem. Mater.* **2008**, *20*, 531–539.
50. Forster, T. Excimers. *Angew. Chem., Int. Ed. Engl.* **1969**, *8*, 333–343.
51. Marcano, D. C.; Kosynkin, D. V.; Berlin, J. M.; Sinitskii, A.; Sun, Z. Z.; Slesarev, A.; Alemany, L. B.; Lu, W.; Tour, J. M. Improved Synthesis of Graphene Oxide. *ACS Nano* **2010**, *4*, 4806–4814.
52. Wang, Z.; Huang, P.; Bhirde, A.; Jin, A.; Ma, Y.; Niu, G.; Neamati, N.; Chen, X. A Nanoscale Graphene Oxide-Peptide Biosensor for Real-Time Specific Biomarker Detection on the Cell Surface. *Chem. Commun.* **2012**, *48*, 9768–9770.
53. Cano, M.; Khan, U.; Sainsbury, T.; O'Neill, A.; Wang, Z.; McGovern, I. T.; Maser, W. K.; Benito, A. M.; Coleman, J. N. Improving the Mechanical Properties of Graphene Oxide Based Materials by Covalent Attachment of Polymer Chains. *Carbon* **2013**, *52*, 363–371.
54. Salavagione, H. J.; Gomez, M. A.; Martinez, G. Polymeric Modification of Graphene through Esterification of Graphite Oxide and Poly(vinyl alcohol). *Macromolecules* **2009**, *42*, 6331–6334.
55. Martin, R. B.; Qu, L.; Lin, Y.; Harruff, B. A.; Bunker, C. E.; Gord, J. R.; Allard, L. F.; Sun, Y. P. Functionalized Carbon Nanotubes with Tethered Pyrenes: Synthesis and Photophysical Properties. *J. Phys. Chem. B* **2004**, *108*, 11447–11453.
56. Wang, D.; Ji, W. X.; Li, Z. C.; Chen, L. A Biomimetic "Polysoap" for Single-Walled Carbon Nanotube Dispersion. *J. Am. Chem. Soc.* **2006**, *128*, 6556–6557.
57. Marek, S. R.; Conn, C. A.; Peppas, N. A. Cationic Nanogels Based on Diethylaminoethyl Methacrylate. *Polymer* **2010**, *51*, 1237–1243.
58. Yi, G. S.; Chow, G. M. Water-Soluble $NaYF_4$:Yb,Er(Tm)/$NaYF_4$/Polymer Core/Shell/Shell Nanoparticles with Significant Enhancement of Upconversion Fluorescence. *Chem. Mater.* **2007**, *19*, 341–343.
59. Ku, K. H.; Kim, M. P.; Paek, K.; Shin, J. M.; Chung, S.; Jang, S. G.; Chae, W.-S.; Yi, G.-R.; Kim, B. J. Multicolor Emission of Hybrid Block Copolymer−Quantum Dot Microspheres by Controlled Spatial Isolation of Quantum Dots. *Small* **2013**, *9*, 2667–2672.
60. Geng, J.; Zhou, L.; Liu, B. Graphene Oxide Enhanced Fluorescence of Conjugated Polyelectrolytes with Intramolecular Charge Transfer Characteristics. *Chem. Commun.* **2013**, *49*, 4818–4820.
61. Singh, G.; Choudhary, A.; Haranath, D.; Joshi, A. G.; Singh, N.; Singh, S.; Pasricha, R. ZnO Decorated Luminescent Graphene as a Potential Gas Sensor at Room Temperature. *Carbon* **2012**, *50*, 385–394.
62. Lim, J.; Yang, H.; Paek, K.; Cho, C. H.; Kim, S.; Bang, J.; Kim, B. J. "Click" Synthesis of Thermally Stable Au Nanoparticles with Highly Grafted Polymer Shell and Control of Their Behavior in Polymer Matrix. *J. Polym. Sci., Part A: Polym. Chem.* **2011**, *49*, 3464–3474.
63. Ferguson, C. J.; Hughes, R. J.; Nguyen, D.; Pham, B. T. T.; Gilbert, R. G.; Serelis, A. K.; Such, C. H.; Hawkett, B. S. *Ab Initio* Emulsion Polymerization by RAFT-Controlled Self-Assembly. *Macromolecules* **2005**, *38*, 2191–2204.
64. Kim, H. J.; Paek, K.; Yang, H.; Cho, C. H.; Kim, J. S.; Lee, W.; Kim, B. J. Molecular Design of "Graft" Assembly for Ordered Microphase Separation of P3HT-Based Rod-Coil Copolymers. *Macromolecules* **2013**, *46*, 8472–8478.